6.7 Preliminary analysis of the Goshen County tornadic supercell on 5 June 2009 during VORTEX2 using EnKF assimilation of mobile radar and mesonet data

JAMES MARQUIS*, YVETTE RICHARDSON, PAUL MARKOWSKI,
Department of Meteorology, Pennsylvania State University, University Park, PA
DAVID DOWELL,
National Center for Atmospheric Research, Boulder, CO
JOSHUA WURMAN, KAREN KOSIBA, AND PAUL ROBINSON
Center for Severe Weather Research, Boulder, CO

1. Introduction

The storm intercepted by VORTEX2 facilities on 5 June 2009 in Goshen County, Wyoming, is likely the most thoroughly observed tornadic supercell to date. Dual- or single-Doppler winds and thermodynamic data from several in situ surface platforms were collected during all stages of the tornado lifecycle. Such data sets are currently being examined in the contexts of tornadogenesis, maintenance, and dissipation, and for other storm-scale topics. Though these data sets provide valuable clues regarding the roles that certain mesocyclone-scale processes play in various aspects of tornado behavior with unprecidented spatial resolution, the dual-Doppler wind syntheses collected on this day only cover a roughly 20×20×3–4km volume of the storm, and only surface thermodynamic observations are available. Therefore, the roles in tornado formation played by storm- or mesocyclone-scale features located several kilometers away from or above the tornado are subject to speculation. Furthermore, no dual-Doppler data are available during the final 15 minutes of the lifecycle of the tornado, making a quantitative analysis of processes involved with tornado maintenance and decay difficult.

This study aims to expand the amount of three-dimensional wind and thermodynamic data available in the 5 June 2009 case by assimilating single-Doppler winds collected by the Doppler on Wheels mobile radars (DOWs; Wurman et al. 1997) and surface thermodynamic and kinematic observations collected by the NSSL mobile mesonets (Straka et al. 1996) into a numerically-modeled supercell storm using the ensemble Kalman filter method (EnKF; e.g., Snyder and Zhang 2003; Dowell et al. 2004). Our preliminary ensemble-mean analyses are compared to dual-Doppler wind syntheses and surface observations to assess their quality. The value of these EnKF analyses is demonstrated in this paper by showing the three-dimensional structure of the rear-flank downdraft and multiple gust fronts where and when dual-Doppler data are not available. Ultimately, our final analyses will be used to support companion studies analyzing various aspects of tornado behavior in the 5 June 2009 supercell (e.g., presentations in this session by Kosiba et al. and Richardson et al.) by evaluating, 1) the origin and evolution of possible multiple rear-flank downdraft surges and their attendant gust fronts, 2) the relationship between mid- and upper-level processes and surface features, and 3) the sources of near-surface rotation throughout the lifecycle of the tornado through the use of parcel trajecory analysis, circulation budgets, and an examination of three-dimensional vortex lines that extend beyond the range of available dual-Doppler data.

*Corresponding author address: James Marquis, Department of Meteorology, Pennsylvania State University, 503 Walker Building, University Park, PA 16802; *e-mail*: jmarquis@met.psu.edu.

2. Method

An ensemble of 50 storms is simulated using the WRF-ARW model. Our current analyses are produced using a time step of 4 s, a horizontal grid resolution of 1.0 km, and a stretched vertical grid with $\Delta z \sim 80$ m near the ground and ~ 2 km near the top of the domain (20 km ASL). Model grid dimensions are 140 $\times$ 75 $\times$ 40 grid points. A Lin et al. (1983) ice microphysics scheme is used with a graupel density of 900 kg m^{-3} and a Marshall-Palmer intercept of 4×10^3 m^{-4}. We use open lateral boundary conditions and implement a Rayleigh damping layer in the upper-most 5 km of the domain. A homogeneous environment is derived from a proximity sounding collected by a NSSL mobile sounding platform located approximately 40–50 km south-southeast of the updraft at 2155 UTC. The boundary layer temperature profile is modified so that the surface temperature is consistent with mobile mesonet observations in the near-storm inflow environment (Fig 1). Convective updrafts are initiated in each ensemble member 10 min before data assimilation using a random configuration of 10 overlapping warm bubbles placed in an area occupied by the storm. Ensemble spread is maintained throughout the experiments using an additive noise procedure outlined in Dowell and Wicker (2009), with T, T_d, u, and v perturbations of magnitudes 0.5 K and 0.5 m s^{-1} added every 5 minutes to the model fields in areas where radar reflectivity exceeds 25 dBZ_e starting 20 minutes after the start of each experiment (1.0 K and 1.0 m s^{-1} are used prior to this time).

Data assimilation is performed with the NCAR Data Assimilation Research Testbed (DART; Anderson et al. 2009) software. Figure 2 shows the temporal coverage of the observations assimilated. Data are assimilated at 2-min intervals over a 2-hr period. From 2045–2130 UTC, synthetic radar data, generated by translating the data in the first DOW7 radar volume (valid at

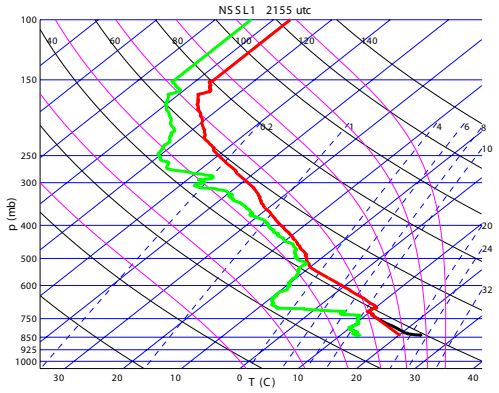

FIG. 1. Skew-T log-P diagram of the NSSL1 2155 UTC sounding representing the homogeneous base state in the EnKF experiments. The red line is the temperature profile modified with surface mobile mesonet temperature observations. The black profile illustrates the unmodified boundary layer temperature profile.

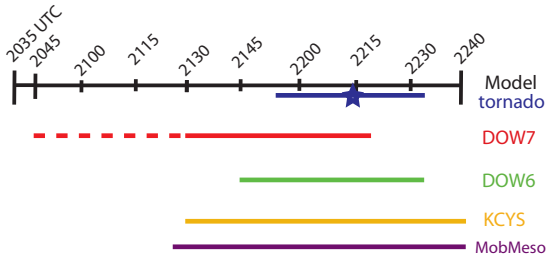

FIG. 2. Timeline of: experiment duration (black bar); approximate tornado duration (blue); and the DOW7 (red), DOW 6 (geen), WSR-88D (orange), and mobile mesonet (purple) data assimilation periods. The dashed red line represents the period of synthesized DOW7 data. The blue star marks the approximate time when the tornado is its most intense.

2130 UTC) to their fictitious prior locations consistent with an average storm motion, are assimilated every 2 minutes. These synthetic data are assimilated because the high spatial resolution achieved by DOW7 appears to aid in spining-up a storm more rapidly than WSR-88D data alone during this period. Prior to assimilation, radar radial velocities are objectively analyzed to conic sections with a horizontal grid spacing of 1 km using a Cressman weighting. Mobile mesonet u and v observations are assimilated when the vehicles are not accelerating significantly. Temperature and dewpoint temperature observations are assimilated when the vehicles are believed to have sufficient aspiration of the thermodynamic sensors. All mobile mesonet observations are assimilated at the lowest model scalar level ($\sim$ 40 m AGL).

3. EnKF verification

Figure 3 compares dual-Doppler DOW wind fields to the ensemble mean kinematic fields at low-levels from two EnKF experiments, one assimilating all single-Doppler velocity observations shown in Fig. 2 and one that also assimilates mobile mesonet observations. Prior to dual-Doppler synthesis, the radial winds from the DOWs are objectively analyzed with a Cressman weighting, and three-dimensional winds are synthesized by iteratively integrating upward from the ground. In order to apply the lower boundary condition below the radar horizon, missing u and v fields below 400 m AGL are set equal to those at 400 m AGL. At both of the times shown in Fig 3, the pattern of vertical velocity along the rear-flank gust fronts and within the rear-flank downdraft in the EnKF experiments closely resembles that produced in the dual-Doppler wind syntheses. The horizontal wind field is quite similar among the EnKF analyses and the dual-Doppler syntheses, as is the placement and evolution of the peak vertical vorticity (both wind retrieval methods have relative peaks at $\sim$ 2201-2205 and 2211-13 UTC, and decreasing magnitudes after 2215 UTC). In general, the wind fields produced in the EnKF analyses are qualitatively similar to those produced in the dual-Doppler analyses regardless if mobile mesonet observations are assimilated, suggesting that assimilating data from multiple radars with different viewing angles appears to adequately represent storm-scale and mesocyclone-scale kinematics.

Figure 4 compares ensemble-mean potential temperature fields produced near the surface in the two EnKF experiments to mobile mesonet potential temperature observations. At 2147 UTC (Fig 4a-c), the ensemble-mean θ deficit in the forward-flank of the storm ($x \sim$ -8 km, $y \sim$ 12 km) more closely resembles observations when mobile mesonet data are assimilated in addition to radar data. However, both EnKF experiments contain near-storm ambient inflow that is warmer than observed (0 $\leq x \leq$ 15 km, $y \sim$ 5 km). These facts suggest that the mobile mesonet observations have the greatest impact near the precipitation core, where ensemble spread is maintained by the additive noise technique described in the method section. Later, at 2201 UTC (Fig 4d-f), we see that assimilating mobile mesonet data increases the peak θ deficit throughout the forward flank region, and decreases the θ deficit in the rear-flank downdraft. The overall pattern, with the warm inflow air and cool rear-flank outflow swirling around the vertical vorticity maximum, is similar in both EnKF experiments. Although it is clear that the assimilation of mobile mesonet surface observations influences the EnKF temperature fields, it is not clear if this influence extends correctly to areas outside the region of mesonet observations. In areas located outside of the precipitation regions, there is disagreement between the ensemble temperatures and the mobile mesonet observations. Future work will pursue methods to optimize the influence of surface temperature observations on the EnKF analyses in areas where ensemble spread is not maintained by the additive noise technique.

4. Storm analysis

Using these preliminary EnKF analyses, we can assess how certain aspects of the storm- and mesocyclone-scale flow that are unsampled by dual-Doppler wind syntheses and surface observations may affect tornadogenesis and maintenance. Figure 5 shows a series of low-level kinematic fields after the dual-Doppler period has ended but before the tornado has dissipated. The low-level mesocyclone begins to weaken substantially by 2225 UTC. Before and after this time, the rear-flank downdraft generally weakens. Interestingly, the gust front separating the

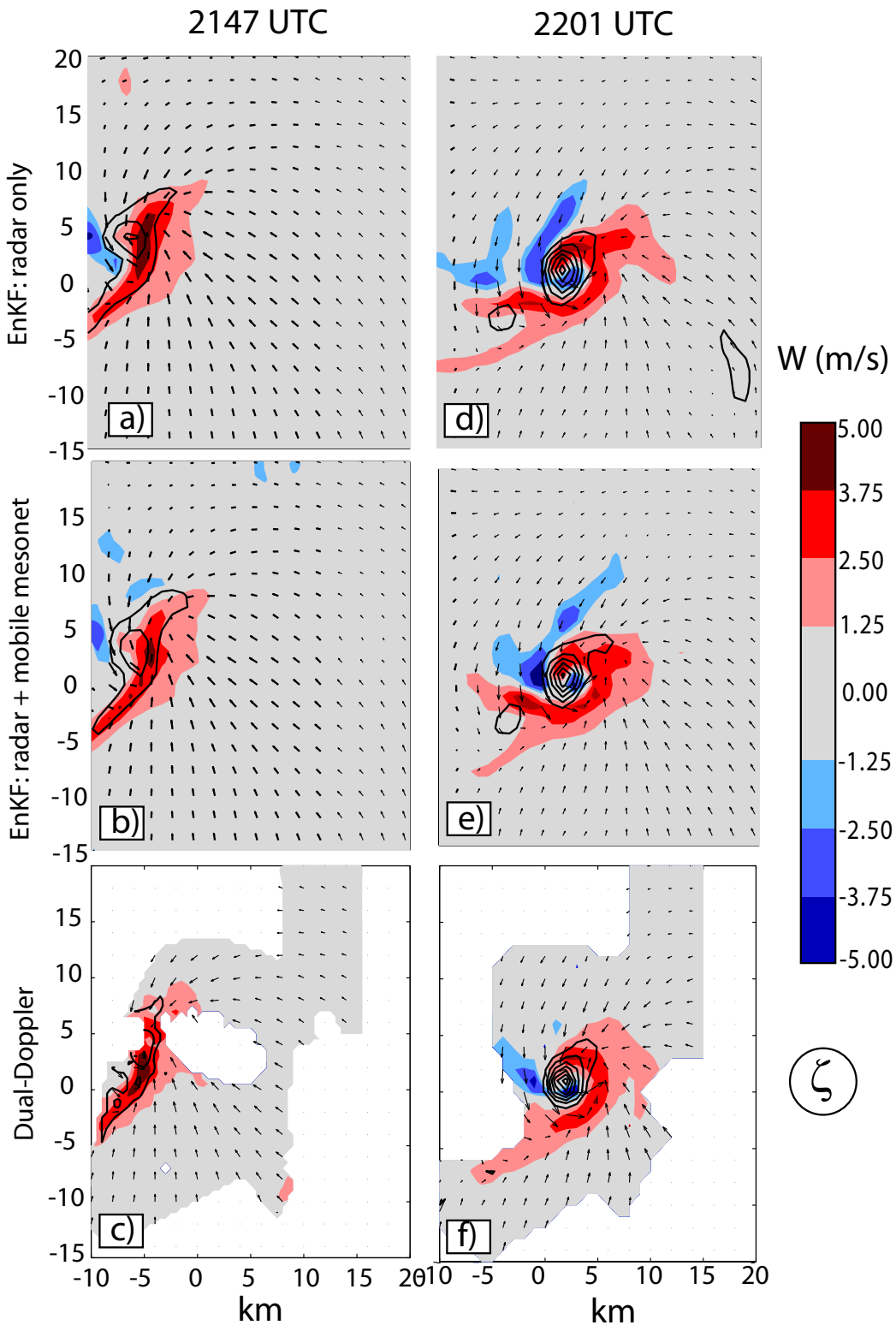

FIG. 3. Ensemble mean vertical motion (shaded), vertical vorticity (contours), and ground-relative horizontal wind (vectors) at z = 400 m AGL at 2147 UTC (left) and 2201 UTC (right) for an EnKF experiment that assimilates only radar velocities (a,d) and one that also assimilates mobile mesonet observations (b,e). The same kinematic fields produced by dual-Doppler wind synthesis are provided in panels c and f.

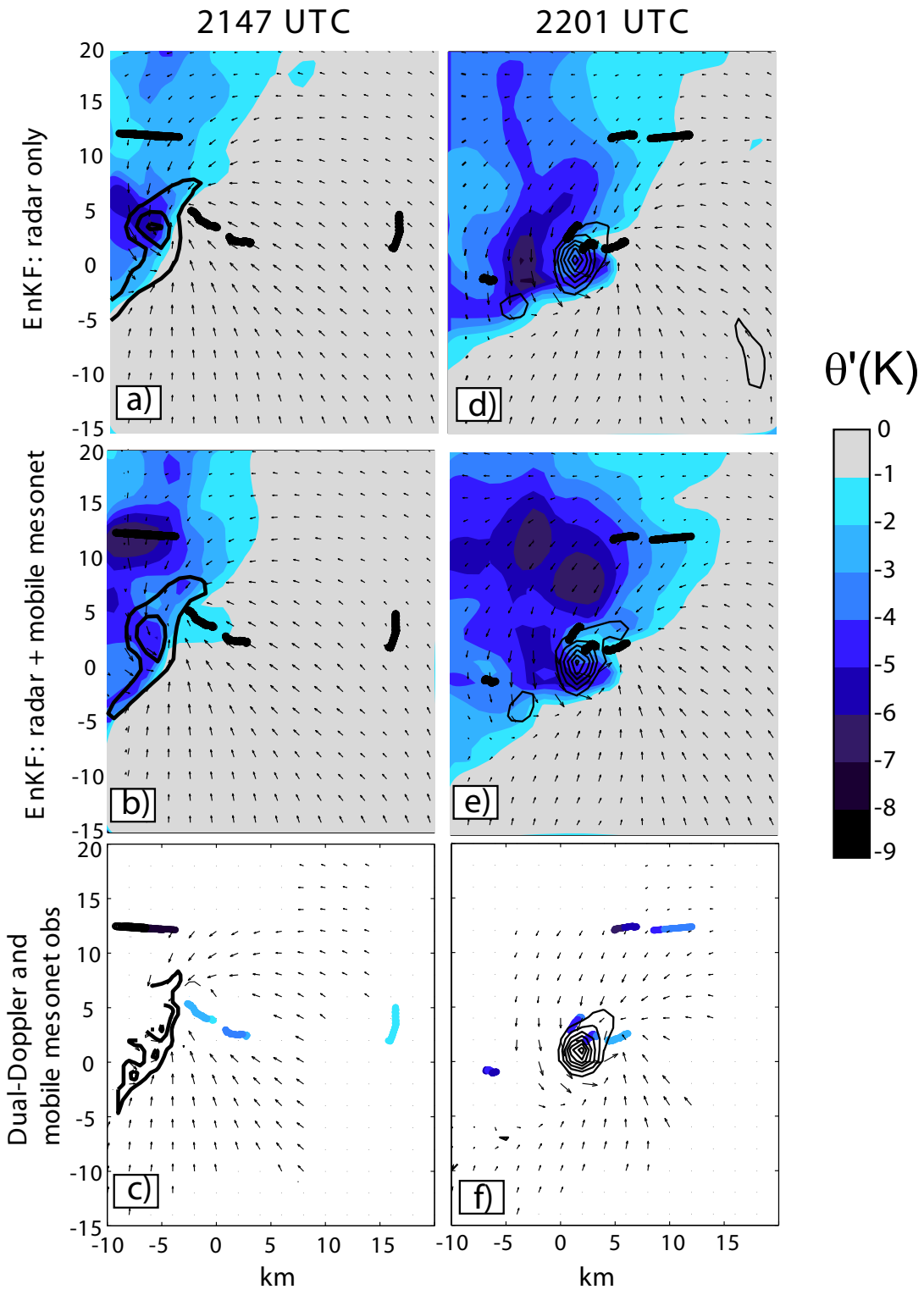

FIG. 4. Same as Fig 3 except the deficit of ensemble mean potential temperature from the base state at z = 50 m AGL is shaded in panels a, b, d, and e. The storm-relative positions of the mobile mesonet vehicles within 1 minute of each analysis time are shown with black streaks. Mobile mesonet surface observations of potential temperature deficit are shown with colored streaks at the vehicle locations.

rear-flank outflow from the ambient inflow does not significantly move relative to the tornado, despite a weakening of the downdraft. This sequence will be examined more thoroughly in future work to determine the relevance of the evolution of these features to tornado maintenance and dissipation.

A possible multiple gust front structure is produced in both the EnKF analyses and in dual-Doppler wind syntheses (bifurcation of the band of upward motion at x = 0, y = -3 km in Fig 3d-f), with the nothernmost gust front branch leading a strong rear-flank downdraft, similar to dual-Doppler observations shown by Wurman et al. (2007). A rear-flank downdraft surge associated with this structure is believed to play a role in the genesis and intensification of this tornado (Kosiba et al., this session). Figure 6 shows horizontal and vertical cross sections slicing through this double gust front structure and the rear-flank downdraft at 2207 UTC. The downdraft has a depth of about 7 km, with a peak intensity of about -8 – -9 m s^{-1} near 5 km AGL. The upper half of the downdraft core resides in a layer of strong updraft-relative wind (upper panel in Fig 6), consistent with Nelson (1977), Barnes (1978), Lemon and Doswell (1979), and others (summarized by Markowski, 2002), who deduce mid-upper-level origins of rear-flank downdraft air. In the y–z cross section, the rear-flank gust fronts (located at y = 18 and 24 km at z = 300 m) have opposite slopes such that they merge into one updraft at approximately z = 2.5–3 km AGL (solid green lines in left panel of Fig 6). A weaker band of upward motion at y = 29 km (dashed green line), borders the downdraft on the northern side, giving the rear-flank downdraft the appearance of an isolated downburst that has reached the ground. Streamlines in the y–z cross section are suggestive of outflow air from the downdraft surge that rises back up along the rear-flank gust front located at y = 23 km and is recycled back into the downdraft. Streamlines in the x–z cross section indicate that ambient air from the east-southeast rises along the gust front east of the tornado into the primary updraft and exits in the anvil rather than penetrating into the rear-flank downdraft. Future analysis will involve the use of parcel trajectory calculations to confirm these air streams and determine how they may affect vorticity generation near the ground.

Dowell and Bluestein (2002) proposed that tornado maintnance was possible in the McLean, Texas, supercell when the motion of the tornado relative to the primary storm updraft aloft is near zero, keeping it in a favorable area for the generation and enhancement of vertical vorticity. This occurred in the McLean storm when a balance between the magnitudes of the storm-relative inflow and outflow existed near the tornado. Figure 7 illustrates the position of the mid-level updraft relative to the location of the near-surface vertical vorticity maximum from approximately the time of tornadogenesis through the time of tornado dissipation from our EnKF experiment that assimilates radar and mobile mesonet data. The near-surface vertical vorticity maximum is located underneath the western edge of the mid-level updraft at all times in the lifecycle of the tornado. Furthermore, the position of the rear-flank gust front (found by tracing the band of upward motion at z = 300 m AGL; blue lines in Fig 7) advances only slightly relative to the near-surface vorticity maximum. These observations suggest that the relative magnitudes of the upraft-relative horizontal inflow and outflow near the tornado did not significantly change throughout its lifecycle (despite a weakening rear-flank downdraft between 2215–2231 UTC; Fig 5), and that processes governing tornado maintenance may be more complicated than a gross imbalance between them in this storm.

5. Summary and Future work

This paper outlines a preliminary EnKF analysis of the 5 June 2009, Goshen County, Wyoming, tornadic supercell that assimiliates Doppler on Wheels, WSR-88D, and mobile mesonet observations. The EnKF kinematic analyses are quite similar to three-dimensional dual-Doppler wind syntheses available at certain times in the lowest few kilometers of the storm, possibly verifying the realism of the simulation. Examination of the kinematic fields permits an analysis of certain storm- and mesocyclone-scale properties of the supercell that are not attainable from dual-Doppler wind syntheses or from data collected only at the surface. For example, we see that the low-level mesocyclone travels along with the mid-level updraft throughout the lifecycle of the tornado, unlike storms that undergo cyclic tornadogenesis and dissipation, and a rear-flank downdraft surge extends up to $\sim$ 7 km AGL, producing a multiple gust front structure that may be important to tornado formation and intensification. Future analysis of storm- and mesocyclone-scale dynamics using the EnKF kinematic fields produced with a model resolution of 500 m will include the use of parcel trajectory calculations and circulation budgets to evaluate the source of rotation near the ground.

As expected, the near-surface EnKF thermodynamic fields more closely resemble mobile mesonet observations in the EnKF experiment that assimilates them than in the experiment that only assimilates radar velocities. However, it is not clear if the details of the thermodynamic fields in the cold pool far from the locations of the mobile mesonet observations and near the locations of the mesonet observations that are located outside of the precipitation regions are accurate. Future experiments will test the sensitivity of the thermodynamic fields to the choice of cloud microphysics schemes, including a dual-moment scheme, and a hetereogenous base state (Dowell et al. 2010). We also will investigate methods to increase the effectiveness of assimilated surface observations in areas outside of the high-reflectivity regions, where our additive noise technique does not maintain ensemble spread throughout the experiment.

Acknowledgments. The EnKF experiments were performed using NCAR CISL supercomputing facilities with the Data Assimilation Research Testbed (DART) and WRF-ARW software. We would like to thank the writers and support staff of these facilities, especially Nancy Collins and Chris Snyder. We would also like to thank all VORTEX2 crew for their dedication while collecting data on 5 June 2009.

This research is funded by NSF grants: NSF-AGS-0801035, NSF-AGS-0801041. The DOW radars are NSF Lower Atmospheric Observing Facilities supported by NSF-AGS-0734001.

REFERENCES

Anderson, J., T. Hoar, K. Raeder, H. Liu, N. Collins, R. Torn, and A. Avellano, 2009: The Data Assimilation Research Testbed: A community facility. *Bull. Amer. Meteor. Soc.*, **90**, 1283–1296.

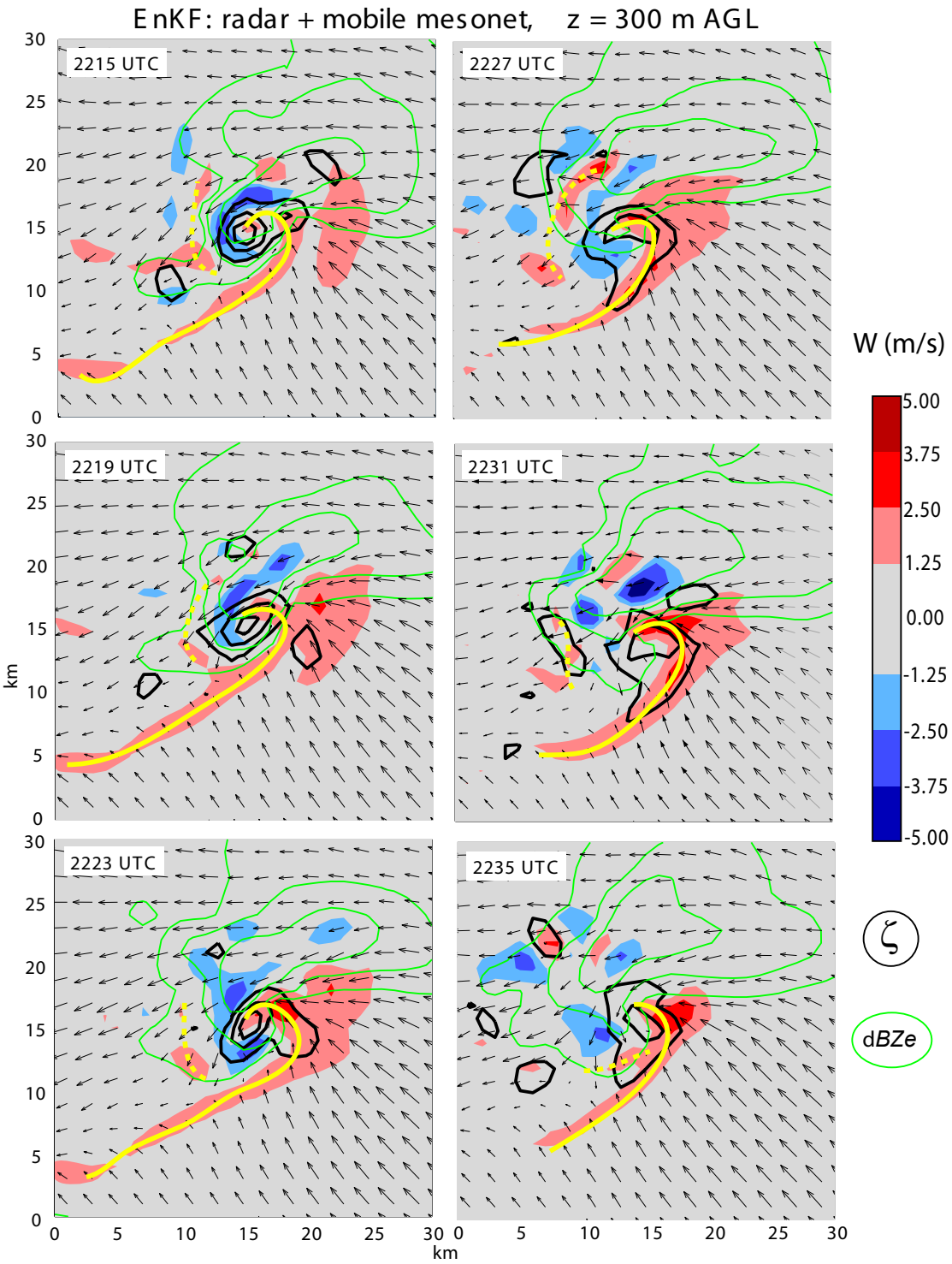

FIG. 5. Same as Fig 3e except at z = 300 m AGL at 2215, 2219, 2223, 2227, 2231, and 2235 UTC. Radar reflectivity computed from model precipitation is contoured in green. Surface gust fronts are traced with yellow lines. Dashed yellow lines indicate possible secondary gust fronts. Vector fields are horizontal winds relative to the mid-level updraft.

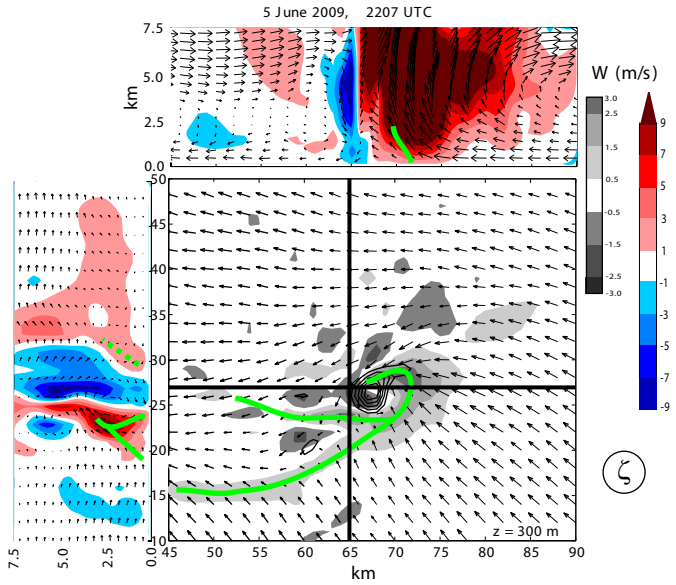

FIG. 6. Ensemble mean vertical velocity (shaded), storm-relative horizontal wind (vectors), and vertical vorticity (contours) at z = 300 m AGL at 2207 UTC from the experiment assimilating radar and mobile mesonet observations. Gust front positions are traced with green lines. Vertical cross sections in the x–z and y–z planes of vertical velocity and storm-relative winds along the bold black lines in the x–y plane are shown in the top and left panels, respectively. Note, there are two different color scales for vertical motion used in the x–y, and x–z, y–z planes.

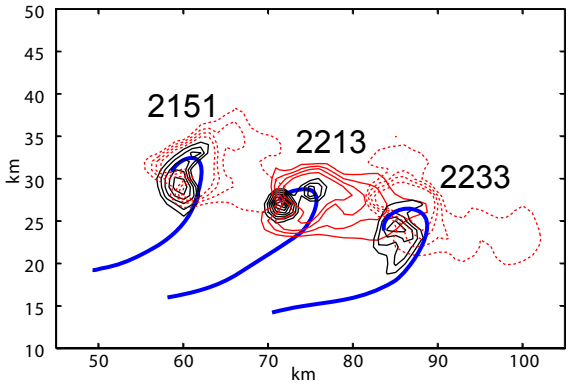

FIG. 7. Ensemble mean vertical motion at z = 5 km AGL (red contours, w = 5, 10, 15, and 20 m/s), vertical vorticity at z = 300 m AGL (black contours), and gust front position at z = 300 m AGL (blue lines) at 2151, 2213, and 2233 UTC from the EnKF experiment that assimilates radar and mobile mesonet observations.

Barnes, S.L., 1978: Oklahoma thunderstorms on 29–30 April 1970. Part I: Morphology of a tornadic thunderstorm. *Mon. Wea. Rev.*, **106**, 673–684.

Dowell, D. C., and H. B. Bluestein, 2002: The 8 June 1995 McLean, Texas storm. Part II: Cyclic tornado formation, maintenance, and dissipation. *Mon. Wea. Rev.*, **130**, 2649–2670.

Dowell, D.C., F. Zhang, L.J. Wicker, C. Snyder, and N.A. Crook, 2004: Wind and temperature retrievals in the 17 May 1981 Arcadia, Oklahoma, supercell: Ensemble Kalman filter experiments. *Mon. Wea. Rev.*, **132**, 1982–2005.

Dowell, D.C., and L.J. Wicker, 2009: Additive noise for storm-scale ensemble data assimlation. *J. Atmos. Oceanic Technol.*, **26**, 911–927.

Dowell, D., G. Romine, and C. Snyder, 2010: Ensemble storm-scale data assimilation and prediction for severe convective storms. Preprints, *25th Conf. On Severe Local Storms*, Denver, CO, Amer. Meteor. Soc., 9.5.

Kosiba K., J. Wurman, P. M. Markowski, Y. P. Richardson, D. Dowell, P. Robinson, and J. Marquis, 2010: The Goshen County, Wyoming, supercell of 5 June 2009 intercepted by VORTEX2: Tornadogenesis phase. Preprints, *25th Conf. On Severe Local Storms*, Denver, CO, Amer. Meteor. Soc., 6.4.

Kosiba K., J. Wurman, P. M. Markowski, Y. P. Richardson, D. Dowell, P. Robinson, and J. Marquis, 2010: The Goshen County, Wyoming, supercell of 5 June 2009 intercepted by VORTEX2: Tornado intensification phase. Preprints, *25th Conf. On Severe Local Storms*, Denver, CO, Amer. Meteor. Soc., 6.5.

Lemon, L. R., and C. A. Doswell, 1979: Severe thunderstorm evolution and mesocyclone structure as related to tornadogenesis. *Mon. Wea. Rev.*, **107**, 1184-1197.

Markowski, P.M., 2002: Hook echoes and rear-flank downdrafts: A review. *Mon. Wea. Rev.*, **130**, 852–876.

Markowski, P.M., Y. Richardson, J. Wurman, K. A. Kosiba, and P. Robinson, 2010: The Goshen County, Wyoming, supercell of 5 June 2009 intercepted by VORTEX2: Pretornadic phase. Preprints, *25th Conf. On Severe Local Storms*, Denver, CO, Amer. Meteor. Soc., P6.6.

Nelson S.P., 1977: Rear flank downdraft: A hailstorm intensification mechanism. Preprints, *10th Conf. On Severe Local Storms*, Omaha, NE, Amer. Meteor. Soc., 521–525.

Snyder, C. and F. Zhang, 2003: Assimilation of simulated Doppler radar observations with an ensemble Kalman filter. *Mon. Wea. Rev.*, **131**, 1663–1677.

Richardson, Y.P., P. M. Markowski, J. Wurman, K. Kosiba, P. Robinson, and J. Marquis, 2010: The Goshen County, Wyoming, supercell of 5 June 2009 intercepted by VORTEX2: Tornado dissipation phase. Preprints, *25th Conf. On Severe Local Storms*, Denver, CO, Amer. Meteor. Soc., 6.6.

Wurman, J., J.M. Straka, M. Randall and A. Zahrai, 1997: Design and development of a portable, pencil-beam, pulsed, 3-cm Doppler radar. *J. Atmos. Oceanic Tech.*, **14**, 1502–1512.